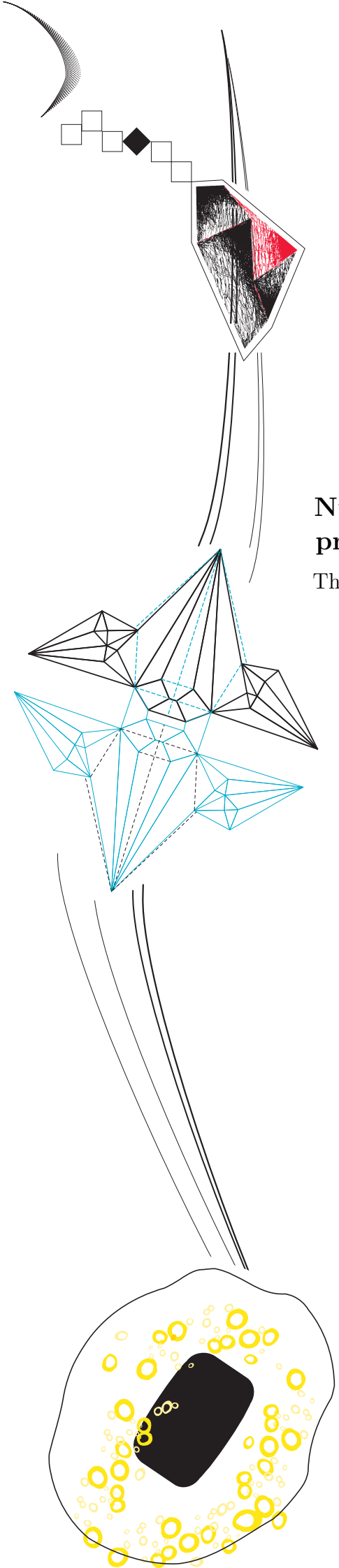

Numerical simulation of ice accretion on a propeller blade

Thomas Laoh (s1012932)

UNIVERSITY OF TWENTE.

Preface

Part of the master curriculum Mechanical Engineering is to do an internship in either an industrial or research environment. The internship is a great opportunity for students to gain insight in the working life after their study and to put their knowledge into practice. This is an excellent chance to not only work at a company for a while, but also to go abroad and live in a different culture. To experience working abroad eventually led to my choice of an internship at CIRA (International Aerospace Research Centre) in Capua, Italy. During the months July to October I have been researching the ice accretion on a propeller of an aircraft numerically. This report describes the process of my research to study ice accretion and an anti-icing system as well.

I would like to thank my supervisor from the University of Twente, Harry Hoeijmakers of the Engineering in Fluid Dynamics group and Giuseppe Mingione from the CIRA Fluid Mechanics department for all their efforts to realize my internship at CIRA. Furthermore, I would like to thank Francesco Petrosino for his close guidance during my research and always being able to answer questions when possible. My time at CIRA was very pleasant and the ambiance and experiences very useful for my future job(s) and studying.

Thomas Laoh

November 2015, Utrecht

Contents

1 Introduction **4**

2 Literature study **5**

3 First aerodynamic simulations **7**

4 Propeller 2D method **11**

5 Full propeller analysis **18**

6 Three dimensional check **28**

7 Conclusion **31**

1. Introduction

Icing on aircrafts is known to be a problem for a long time and many studies have been conducted to determine the effects of this phenomenon. These studies focused on ice accretion and the effects on the plane of the accumulated ice. Over the years many methods have been designed to de-ice or prevent ice accretion on a plane. These methods differ for the different parts of the plane. So far, most research has been done on the wing. Ice accretion on a propeller will reduce the aerodynamic performance of the propeller meaning the thrust will reduce significantly. This could eventually mean that the plane is not able to maintain the velocity needed to stay airborne.

The goal of this study will be: *To perform an assessment of methods for propeller ice protection and to perform a case study for propeller ice accretion and ice protection design.*

The set up of this research is to first get acquainted and understand the numerical approaches used to predict icing on aircraft geometries. After which the best method is searched to make a simplified simulation of the propeller by attempting to make the simulation two dimensional in Chapter 4. The best method found is then used to fully asses the propeller in Chapter 5. These simulations are then verified with simulations from a three dimensional flow field in Chapter 6.

Nomenclature

SLD	Supercooled Large Droplet
LWC	Liquid Water Content
MVD	Median Volumetric Diameter
rpm	rounds per minute
W	Watt
c	chord
Ω	Rotational velocity (rad/s)
T	Temperature (K)
ρ	Density (kg/m^3)
U	Velocity (m/s)
r	radius (m)
a	Speed of Sound (m/s)
U_∞	free stream velocity

2. Literature study

In-flight icing could occur when an aircraft flies in a temperature range between $-40°C$ and $0°C$. In these conditions Supercooled Large Droplets (SLD) can form from small droplets, below these temperatures SLD can not exist. These droplets are unstable and when contact is made with an airfoil or propeller, they immediately freeze to the surface. The first ice accretion is usually on the propeller before it is visible on the wing. While freezing the droplets increase in temperature until $0°C$ is reached. When the droplet is not completely frozen after the temperature rise, the remaining fluid will start to run back on the airfoil or on already formed ice. The shape of the ice is dependent on the liquid water content (LWC), the droplet diameter, the airspeed and ambient temperature. For low temperatures (-40 to $-10°C$), low airspeed and low LWC, the ice immediately freezes and forms 'Rime ice'. It alters the shape of the airfoil changing the aerodynamic characteristics and adding weight, possibly bringing it airfoil out of balance. At higher temperatures (-18 to $0°C$), higher airspeed and high LWC, the forming of 'Glaze ice' is more likely. Glaze ice has a completely different profile than the airfoil, forming for example a double horn. These glaze ice shapes form a danger as they significantly change the aerodynamic performance. Examples of both ice forms can be found in figure 2.1.[1, 2, 3]

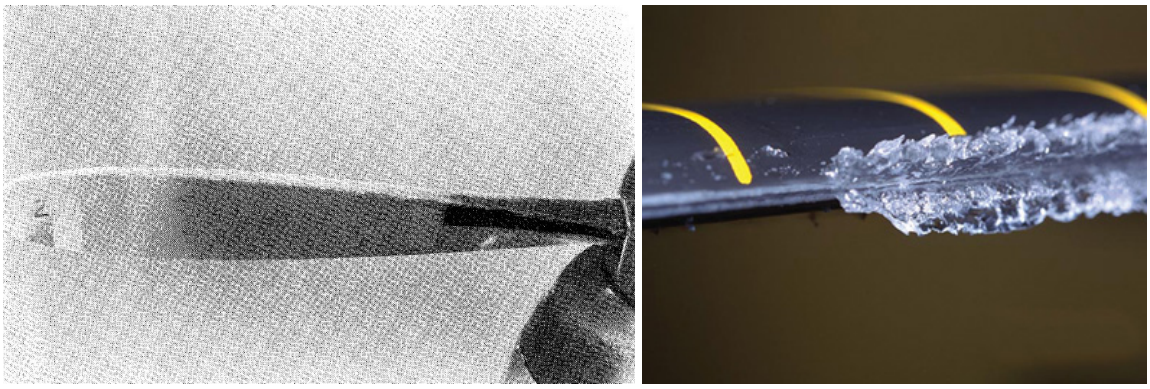

(a) Rime ice (b) Glaze ice

Figure 2.1: *Two different types of ice on a propeller blade*

Over time systems have been designed to remove the ice (de-ice), or to prevent ice accretion (anti-ice) to airfoils. Not all of these are applicable on propellers as they are designed for larger (stationary) surfaces. For propeller blades, only two methods are found to be applicable. Firstly, there are a fluid based 'weeping wing' systems, where alcohol or another freezing point depressant is distributed along the propeller by a discharge nozzle or slinger ring. The nozzle distributes the fluid at the centre on the leading edge. The fluid is then distributed along the leading edge by the centripetal force through grooves in the boot. Advantages of this system are that the airfoil contour can be retained. No runback ice or any residual is left after the system is actuated. The system has a low power demand. Some drawbacks of this system are that it can only carry a limited supply, so it will need to be refilled. The liquid system is least effective when the adhesive bond is the greatest, with low LWC, low temperatures and low MVDs. Lastly, if the turboprop aircraft uses engine bleed air, the liquid cooling is not possible as it can cause harmful vapours inside the cabin.

A second option is to heat the surface with electrical heating pads. Power generated by the engine is

used to transfer power along wires to a heat a conductive layer of insulation on the airfoil. The electrical energy should then be applied either continuously to keep the profile clean of ice or intermittently to loosen and shed the accumulated ice. To maintain an ice free airfoil, the temperature of the surface should be continuously above the freezing point, it should be checked however that no runback water can freeze further on the propeller. The main benefit of this system is the simplicity. Also, the response time of the system is very short compared to the other systems. A disadvantage of this system is that it is power consuming, especially when evaporative anti-icing is desired. A quick search in available systems learns that the power used for these kind of anti-icing systems is around 15 kW.

Other methods which work fine on a wing or stationary part are not applicable for propellers. One of these methods is hot gas de-icing. It is found to be an effective way to transfer heat to the blade by using bleed air of the engines transferred to the surface through small holes. However, this way of transferring heat remains limited for wing surfaces and is thus not applicable on the desired propeller. Also, the use of pneumatic boots (with bleed air) is not applicable. [2, 3, 4, 5, 6, 7]

Some experiments

Some tests have already been done with icing on a propeller, for example by Dumont et al. who conducted an experiment based on a MU-2B propeller. They state that mainly the performance loss of the propellers has been documented, but the accretion characteristics are not. In their experiment they measured the engine rpm, torque, blade angle, boot voltage(s), thrust, wind speed and temperature. They were not able to measure the exact LWC and MVD during the tests, but calibrated the set up before the experiment. The icing conditions were correspondent to the icing regulations as presented in Appendix C of the federal aviation regulations. These are the conditions to which the aviations systems have to be able to withstand icing to get a safety certification. The velocity profile of the airflow decreased after a span of 75% was reached, this they assumed acceptable. Despite the fact that exact profiles have not been shown in the work of Dumont et.al. they have presented some results about the thickness of the ice on various span widths. They measured the thickness on the leading edge at span widths 28% (just after the icing boot), 50% and 75%. Due to a lack of time they only performed tests with the de-icing device turned on. The resulting ice accretion on the propeller was then measured in thickness at the three mentioned points. The results state that in case of icing, most of the times it was found at the span width of 50% (nearly half of the cases) and a runner up at 28% (one third of the documented data). [8, 9, 10]

Also, research has been done discussing propeller performance using the vortex theory by Busch et al. First they developed numerical code to be able to simulate the propeller performance. After this code was developed they used experimental data from Corson and Maynard, who performed a full scale icing test in 1946, to validate the code. With these experimental results the effect of icing is included. Combining their code to the results of the thrust, power coefficient and the propeller efficiency found by Corson and Maynard gives good icing effect results. After this validation they also try to use the experimental results from (Dumont et al.) to validate the effect of icing on the propeller. They conclude that the properties found numerically for icing are reasonable but can be improved by adding more experimental results between the $25\% - 50\%$ range instead of interpolating. Also, it is stated that differences between experimental and simulated effects might also have occurred due to shedding of ice after the measurements of for example the thrust. Recommending the addition of an ice shedding model could be the solution in predicting an accurate solution of the performance degradation of a propeller. [11, 12, 13]

3. First aerodynamic simulations

For every numerical simulation it must be made sure that the numerical simulations provide realistic results. Therefore, before any propellers are researched, a simulation has been made of airfoils which are shaped quite similar to propellers, for which experimental data is available. These simulations are both run to check the validity of the results for these wings and to learn the process of running these simulations. This chapter will contain information about these trial simulations, the generation of results and the results compared to the experimental results. This is all documented extensively such that the obtained results can be reproduced. [14]

To perform any kind of numerical simulation, a mesh must be made which will be the domain for the flow. To do so, the geometry of the airfoil is loaded into *Ansys ICEM CFD*. These are (x, y)-coordinates from which the airfoil geometry is generated by manually connecting the points to describe the profile. Also, a far field boundary is built, the result is shown in figure 3.1(a).

To set up the mesh of the flow field, a 2D block can be created. The edges of the block are associated with the far field profile (figure 3.1(b)). To be able to make a mesh refinement near important flow features like the leading edge of the profile, the block is then divided into five domains. On the front a domain for the leading edge which has to be fairly fine. Near the upper and lower edge of the airfoil the mesh should also be relatively fine such that a boundary layer can be simulated. The two domains for the wake behind the airfoil do not have any significant influence on the calculations and can thus be relatively coarse further away from the airfoil (figure 3.1(c)).
The sections on the leading edge and the upper and lower side of the airfoil are provided with a hyperbolic spacing of the cells along the profile. Over the whole mesh the spacing of cells is set to become exponentially smaller as it approaches the airfoil. The far field cells will not have changes in velocities, but closer to the airfoil, and especially inside the boundary layer large fluctuations in velocities will occur. Subsequently, the upper and lower sections behind the airfoil are set to increase their spacing exponentially moving away from the profile. This all results in a fine grid near the airfoil, as desired and far away at the far field regions the grid is coarse as shown in figure 3.1(d).

Having created the mesh, the flow field still has to be determined. The program used is *Ansys Fluent*. To do so a couple of extra steps have to be carried out. Firstly, the pre-mesh generated needs to be converted into an unstructured mesh, which is the type of mesh used in *Fluent*. Secondly, the output variables need to be qualified. The solver used is *Fluent_V6* and the common structural solver is *NASTRAN*. Thirdly, the type of boundary conditions need to be provided. The far field is set to be a *pressure-farfield*, the airfoil is set as *wall* and the internal mesh is set as *fluid*. Lastly, the output needs to be written as a 2D simulation without any scaling.

To finally begin with the simulation of the flow field, the mesh is opened in *Fluent*. To perform this simulation the program is opened in a 2D - double precision mode. Firstly, the mesh quality is checked and the domain reordered to reduce bandwidth. The solution to be made is a steady, planar, pressure-based solution. Making use of the 1-equation Spalart-Allmaras viscous model which is set to be strain/vorticity based. Subsequently, the properties of the air as fluid are set to be an ideal gas, where the Sutherland Law is used as viscosity model. Next up the boundary conditions are set as presented in the experimental data, such that a comparison can be made between the computational model and the experimental results. The data for the practice geometries is presented in table 3.1.[14, 15]

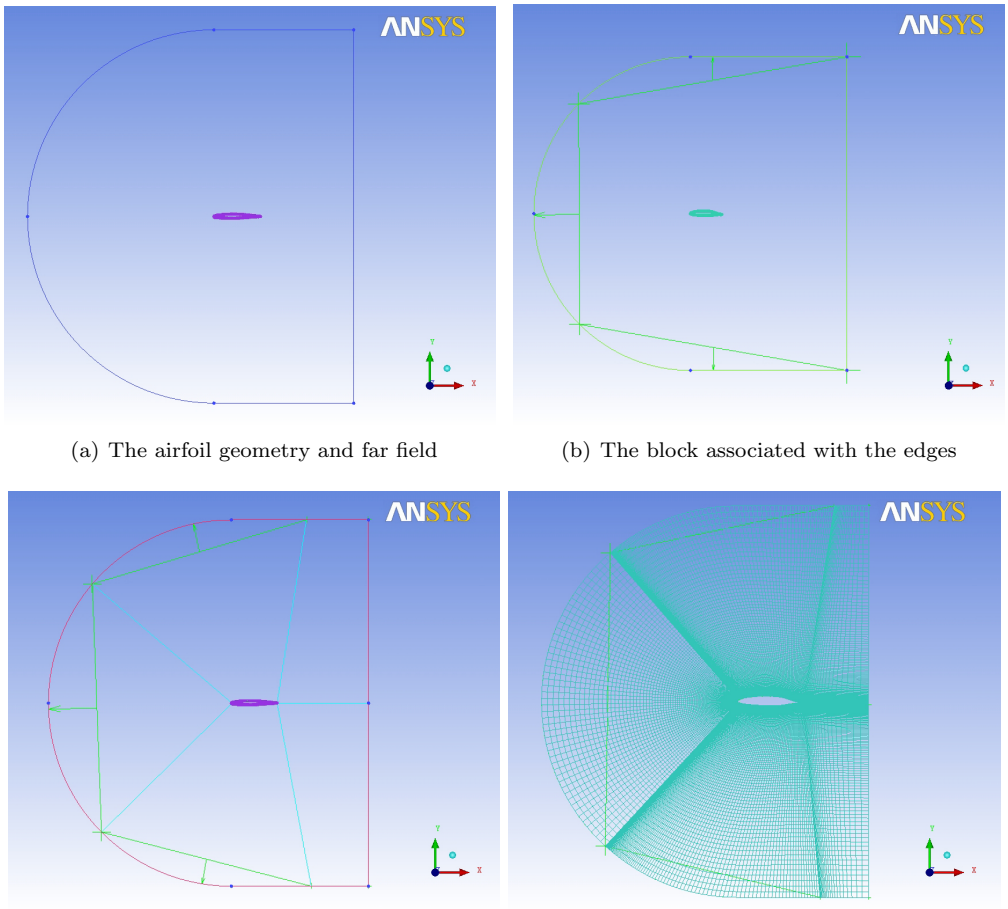

(a) The airfoil geometry and far field

(b) The block associated with the edges

(c) Splitting the block in five different blocks

(d) The mesh of the flow field

Figure 3.1: *Creating a mesh using* ANSYS ICEM CFD

Property	**GLC-305**	**NFL-414**
Static temperature T	263.6 K	267.3 K
Velocity U_∞	128.6 m/s	66.9 m/s
Mach number M_∞	0.396	0.204
Chord c	0.9144 m	0.9144 m
Angle of Attack	1.5°	2°
LWC	0.5 g/m^3	0.54 g/m^3
MVD	15 μm	20 μm
Spray time	472 s	1350 s

Table 3.1: *Experimental flow properties of both airfoils.*

Now the flow field corresponding to the experimental set up can be determined. The Solution method used is a coupled scheme and apart from the *Fluent* defaults, the Modified Turbulent Viscosity is set to Second Order Upwind. Convergence of the solution is not searched in the residuals of the continuity, the velocities or the energy equation as these converge too fast. Therefore, the lift and drag coefficient are also plotted and written and when these converge the solution is assumed converged. Depending on, among other things, the Mach number and angle of attack convergence of the solution can already be reached within 100 iterations.

After these calculations, the flow field with corresponding velocities and pressures are known and can be plotted. An example is shown in figure 3.2. To be able to simulate the icing on the airfoils, the computer code of *Multi-Ice* is used. This program uses the airfoil geometry and the (dimensionless) velocities in the

flow field. At first, to obtain the data needed, the results of the Fluent simulation are written into case and data files. These are then opened using *tecplot 360* to write the data in an *ASCII*-file. Doing this, the velocities are made dimensionless by dividing them with the far field velocity. After this, the icing simulation can finally begin.

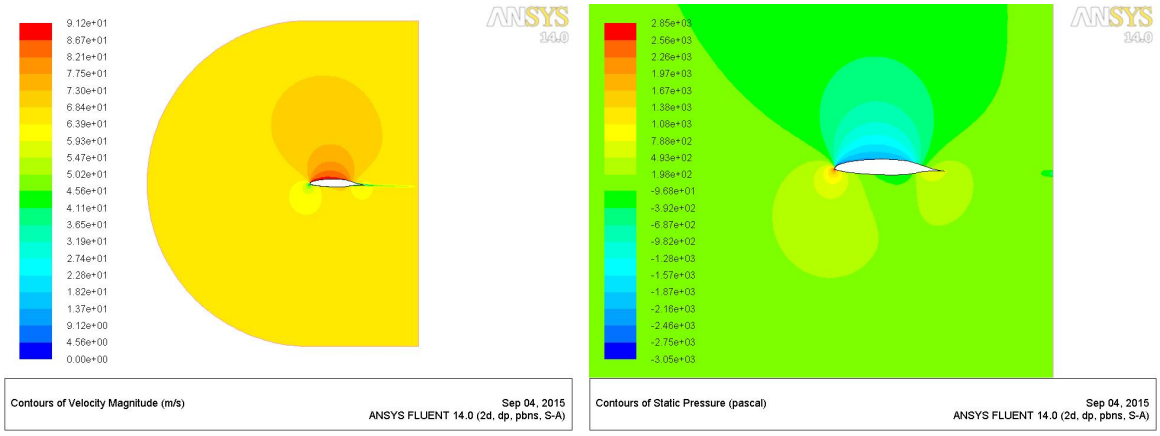

(a) Velocity magnitude (b) Static pressure

Figure 3.2: *Plots of the NFL-414 flow field characteristics.*

At first the airfoil geometry and the flow field are read into *Multi-Ice*. Subsequently, the corresponding conditions of the flow field are set, again. The reason for this is that the data files created in *Fluent* and altered with *tecplot* do not contain data of the temperatures and droplets. The simulation ran is then a *Field method - Predictor* run. After running the *Multi-Ice* simulation and with the use of *MATLAB* the data of the iced airfoils have then been layered over the presented experimental data to be able to give a comparison of both simulations. The results of the icing on over the clean profile are presented in figure 3.3. [16]

Now that the simulation has been layered over the experimental data, the results can be compared. Firstly, the *GLC-305* simulation (figure 3.3(a)) is discussed. It can be noticed is that the simulation has about a similar ice thickness as the experimental results have, only the horn is located lower on the leading edge. Especially the lower horn almost exactly corresponds to the results of the *LEWICE* simulations, whereas the upper horn is clearly better simulated by the other simulation type. However, again the thickness of the ice profile is about the same in all results. Finally, one thing stands out in this simulation. This is the ice glitching through the surface of the airfoil, which of course should not be possible. When the data is extracted from Fluent to Multi-Ice, the geometry file for the airfoil is not documented with an increasing s-coordinate and has to be manually sorted. There was a minor error which resulted in the glitch. This is visible in figure 3.4, here it shows that the glitch is indeed on that same location.

Secondly, the results of the *NFL-414* simulation, which are presented in figure 3.3(b), show a general agreement in the shape of the ice. However, the thickness is much less than found in the experimental results. This thickness, amount of ice and especially runback ice is less in the simulation than one would expect. As the temperature is in the range of $0 - 10°C$, a lot of runback ice is expected according to the literature study. In the experimental results the glaze ice is much thicker than one would expect as well but there is also clearly runback ice present. The simulations of *LEWICE* seem to correspond better to this simulation, apart from one peak which is more appropriately simulated in *Multi-Ice*. Probable cause for the reduced ice thickness is the temperature range, as the code works better with colder temperatures to compute the icing. When water does not completely freeze, the *Multi-Ice* code does not let it flow to other regions, but build up on the same location. This is an explanation for the much smaller amounts of ice and the absence of runback ice in this simulation.

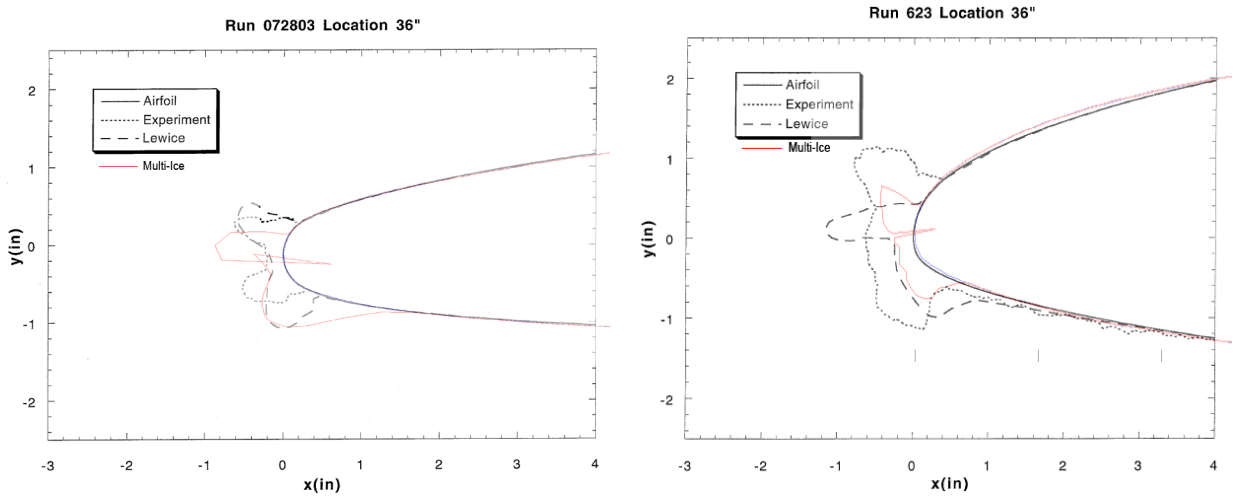

(a) GLC-305 (b) NFL-414

Figure 3.3: *The icing simulation with the use of Multi-Ice (coloured), compared with the experimental data and NASA's LEWICE simulation. Using the data from table 3.1*

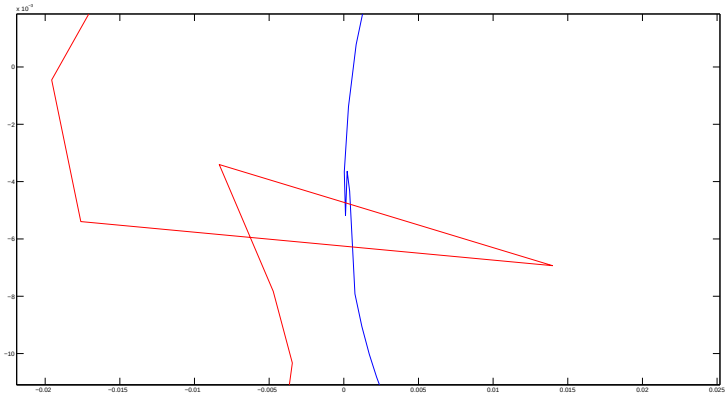

Figure 3.4: *The GLC-305 airfoil zoomed in on the leading edge*

4. Propeller 2D method

Knowing the methods of analysing a flow around an airfoil, an analysis can be made of a flow around the propeller of a turboprop aircraft. The propeller analysed does contain four propeller blades and rotates at 420 rpm. This system is placed in flow of 102.89 m/s along the x-axis, a 0° angle of attack on the set up. A graphical representation of the system - containing the four propeller blades (red), the domain in which the flow field is calculated (yellow cylinder) and the wakes (blue) which are not further used during this analysis - is shown in figure 4.1.

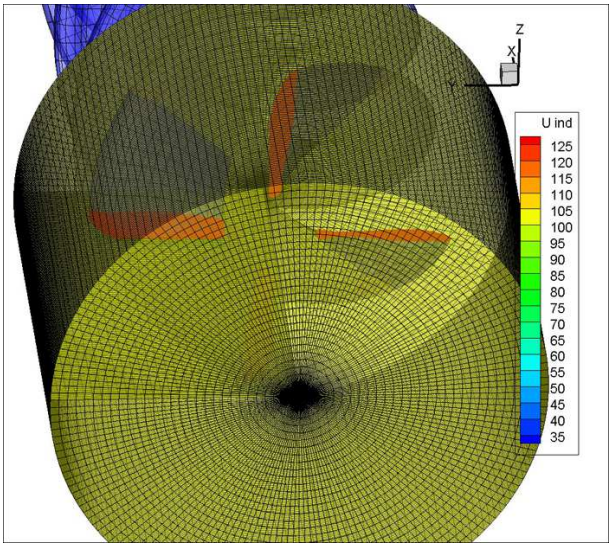

Figure 4.1: *The numerical domain for the flow field (yellow), the propellers(red), propeller wakes (blue)*

The solution provided is given in nine different time steps, as the flow around the propeller blade could vary during the rotation. Furthermore, a 2D solution is sought for an obvious 3D problem. Where all previous analyses were made of airfoils, the propeller blades do not only move in the free stream direction, the blades are also rotating. This gives an extra velocity component in radial direction. Moreover, near the tip of the propeller blade downwash will be present, creating vortices in the flow field. Near the nacelle of the propeller (the centre of the blades) the flow will also be disturbed and can not be assumed 2D. Lastly, the propeller blade has a curl. To be able to make a 2D solution of this problem, the propeller is cut into multiple slices. This approximates the different curls at different speeds. The geometry of a propeller blade is shown in figure 4.2.

The unsteadiness of the solution due to the rotating is dealt with by taking the a slice the same blade section of all time steps. This has been realised by rotating the complete grid to the same position. Such that the first propeller blade with corresponding flow field is rotated back with α degrees using rotation-around the x-axis. This way the same same propeller blade will be directed along the z-axis making it able to obtain the exact same slice each time. The equations used are given in equation 4.1 (for a 45° rotation). The same rotation matrix can be applied to the velocity components. This way the flow field of different time steps can be properly evaluated. To deal with the 3D effects near the nacelle and of the downwash at the propeller tip, they have been cut off the geometry of the propeller blade.. To be certain the measured flow is not influenced by this three dimensional effects, the slices have not been taken too

close to the edge. The locations of the slices are shown in figure 4.2 as the red lines (only z1 to z4 are used in the current analysis).

$$\begin{aligned} x' &= x \\ y' &= y\cos\left(\frac{45\pi}{180}\right) - z\sin\left(\frac{45\pi}{180}\right) \\ z' &= y\sin\left(\frac{45\pi}{180}\right) - z\cos\left(\frac{45\pi}{180}\right) \end{aligned} \tag{4.1}$$

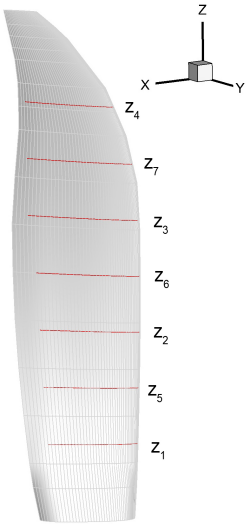

Figure 4.2: *The geometry of the propeller blade, with the shown slices (black lines) and corresponding numbers*

To prove that it does not matter what angle blade has to analyse the flow around on a relative coordinate system, a visual check has been made and afterwards the flow properties were compared in magnitudes. In this flow case the aircraft flies horizontally, this means that the angle of attack for the propeller blades is the same in each location of the cycle. This means the expectation is that the flow will be equal at all locations. Four positions of the blade section at radius $z = 1.95m$ have been presented in figure 4.3. Apart from very little differences the flow is indeed the same. An explanation of the minor differences is found in the rotation of the grids, due to the rotations some grids in the xy-plane become more refined than others, therefore presenting a better interpolated result in the desired direction. The same results are obtained for the other flow properties and sections of the blade, but these are omitted from the report due to the lengthiness.

When the flow is analysed more closely something odd is visible. Figure 4.3 also has the streamlines plotted for the comparison. These streamlines clearly show that the flow does not deflect as much as one would expect. The flow does not seem to comply with the no slip condition as the flow goes straight through the blade. Moreover, the flow due to the rotation of the propeller system does seem to be absent here as the flow is almost entirely horizontal, except for a small disturbance by the blade.

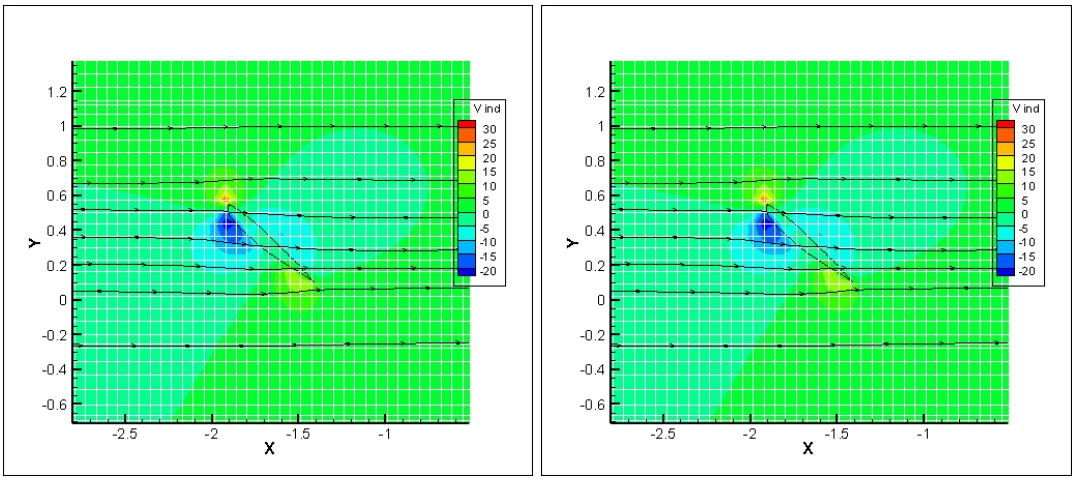

(a) Pitch angle 0˚ (b) Pitch angle 45˚

(c) Pitch angle 90˚ (d) Pitch angle 135˚

Figure 4.3: *The 2D flow field (contour of velocity v in Y direction) around the propeller at a radius of* $z = 1mv$*for different time steps.*

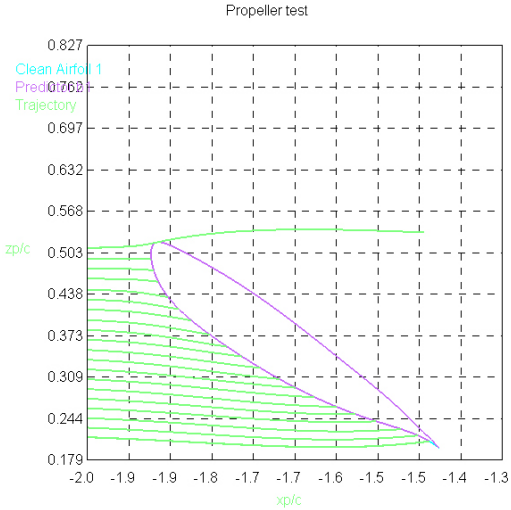

Figure 4.4: *The clean airfoil with ice plotted over it* ($T = 244.7K$, $U_\infty = 102.89m/s$)*, and the limit trajectories.*

Despite the realisation this flow field is not realistic, an analysis has been made in *Multi-Ice*. This is

done to be able to see the accretion on the profile with the current flow. In figure 4.4 is visible that the accretion profile is not at all what is expected. The plot has been made with various accretion times, but in the given flow field no ice is attached to the profile. Also the droplet trajectories confirm that the flow field is not good compared to the expected results, as the droplets (which have a standard MVD of $20\mu m$) should be deflecting around the profile further away from the stagnation point, which is obviously never going to happen as the streamlines of figure 4.3 show.

The previous results are clearly not as what was hoped to achieve. To have at least one proper simulation of this set-up a simulation in *Fluent* has been made. This was done in a similarly to the meshing as performed in the preparatory paragraph (*First aerodynamic simulations*). The profile used was of the propeller blade section $2.5m$ away from the centre of the propeller. Furthermore, the remaining properties, previously unused in the other flow field, to be able to simulate a result which might be possible to compare. These are given in table 4.1. Furthermore, in this simulation use have been made of the apparent speed as shown in figure 4.5. This flow angle is computed by adding the vectors of the speed in horizontal direction and the one causing the speed experienced due to the rotation.

Property	Value
RPM	426
Ω	44.61 rad/s
$\Omega \times r$	111.53 m/s
$U_{\infty x}$	102.89 m/s
a	339.12 m/s
T	286.2 K
ρ	1.190 kg/m^3
$U_{apparent}$	151.73 m/s

Table 4.1: *Properties of the air used to simulate flow field of figure 4.6*

In figure 4.6 it is visible how the streamlines now are tangent to the profile instead of the odd horizontal streamlines as plotted in figure 4.3. This simulation gives a better result regarding the flow near the profile. Now that the flow field has been obtained, it can be used for a computation in *Multi-Ice*. For this simulation, the standard settings regarding temperature, MVD and accretion time are used, as the flow field is computed with the same settings as the previous flow field. Which was generated with a flow above freezing temperature. As the flow will be altered insignificantly due to the temperature difference, this is assumed as a valid simplification.
The shape of the ice accretion is presented in figure 4.7. The ice is accumulating underneath the leading edge of the section blade. There is as seen earlier, a small glitch in the airfoil geometry where two points are not connected properly, resulting in a spike of ice out of (and into) the blade. This means the airfoil geometry should be computed with more care to make sure the geometry is ordered correctly. Below the leading edge is the place where most ice accretion would be expected. On the other hand, this flow simulation assumes the apparent flow as presented in figure 4.5 to be also in this matter in the far field. It needs to be checked, however, if this is a reasonable assumption.

An ideal solution for computing this obvious three dimensional problem in a two dimensional simulation would be when the flow field could be combined, imposing the rotational velocity onto the propeller blade section. To do so, the same mesh can be used as used for the earlier simulation. However, the difference is that from the flow properties of table 4.1 the apparent velocity $U_{apparent}$ is not used any more. The free stream velocity imposed on the pressure-farfield zone, is set to $U_{\infty x}$ with a 0° angle of attack. And the section of the propeller blade is no longer set to be a stationary wall. But it is now to translate with the velocity of $\Omega \times r$ in the positive direction along the Y-axis. This way, the physics which the droplets in the free stream experience should correspond closer to the reality as they are only diverted as they approach the propeller.
In figure 4.8(a) this flow field is shown, where the droplets are carried in the horizontal flow, diverted around the profile. Behind the profile, two vortices appear as the flow fully separates from the profile. Although some effects are visible from the translating of the propeller blade, it must be confirmed using a three dimensional flow field. The level of separation of the flow is however not promising for the validity of

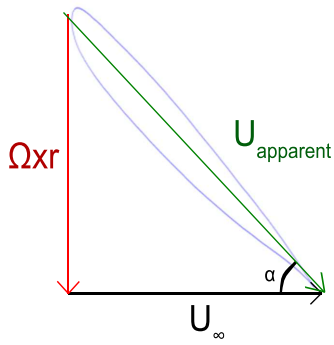

Figure 4.5: *The apparent velocity (green) to the airfoil, combining the Free stream velocity U_∞ (black) and the rotational velocity $\Omega \times r$ (red)*

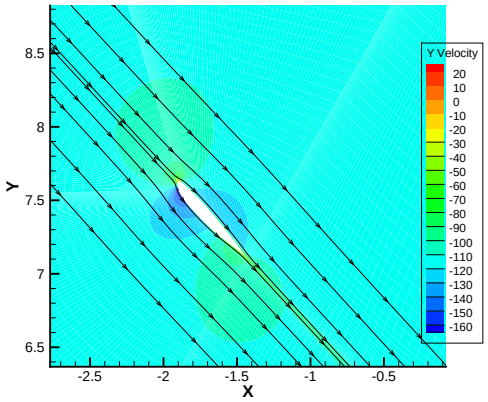

Figure 4.6: *The flow field around the propeller blade with the conditions of table 4.1*

the simulation, as this would mean there is a huge amount of drag inflicted on the propeller. The results regarding the ice accretion with the standard Multi-Ice settings (Table 4.2) are shown in figure 4.8(b). As to be expected, the ice build up is now located much lower than the leading edge. The absence of ice on the leading edge is worrisome, because despite that ice would be expected on the lower side of the propeller, the leading edge should also be fully covered.

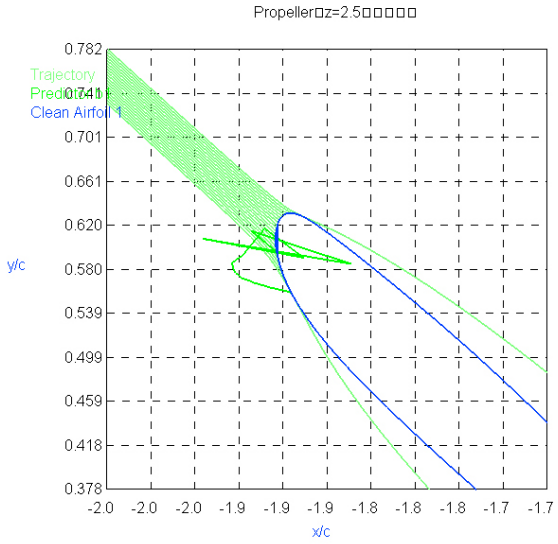

Figure 4.7: *Multi-Ice simulation with the flow field of figure 4.6 and outside temperature* $T = 244.7K$ *and accretion time* $t = 360s$

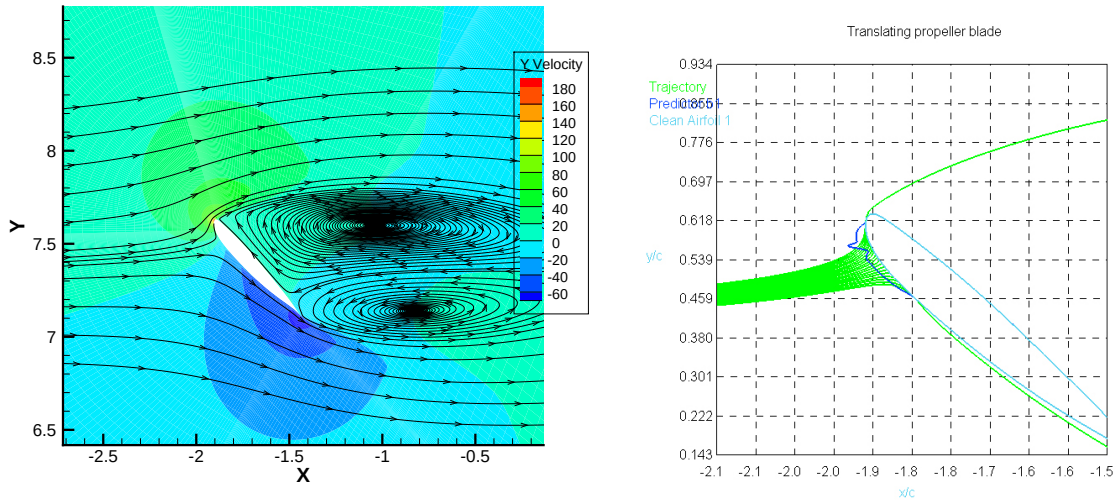

(a) Flow field with induced translation of the propeller blade

(b) Ice accretion profile at corresponding flow as in Table 4.2

Figure 4.8: *The flow field with an induced velocity on the propeller blade and flow properties of 4.1.*

Property	Value
LWC	$1\ g/m^3$
Accretion time	$360\ s$
Air Temperature	$244.7K$
MVD	$20\ \mu m$

Table 4.2: *Standard* Multi-Ice *settings regarding flow properties*

Now that these initial simulations have been made, the choice has been made to further examine the solution using an apparent velocity from the far field. The strongest reason is the doubt of the validity and lack of knowledge present about the solution with the translating section. The droplet size of 20 μm

is evaluated, which are tiny droplets, which will easily follow the flow. Therefore, the assumption is made that the plotted streamlines tangential to the propeller sections are plausible for the droplets to be their trajectory as well. This can hopefully later be confirmed with the use of a (slice of a) three dimensional flow field.

5. Full propeller analysis

To obtain a proper analysis, all simulations are made using the same conditions for creating a flow field. The conditions used are still the same as the original (faulty) three dimensional flow field, as a new three dimensional flow field was promised. The assumption is that the same conditions for generating the flow are used. These conditions are listed in table 5.1. To obtain a view over the whole span of the propeller blade, several sections of the geometry have been used. The sections used are shown in figure 4.2 including the corresponding section numbers. Please not that the bottom of the shown geometry is not the centre of the propeller set. This centre is located close to one meter lower. The distances from the centre of the set of propellers (r) and the corresponding apparent velocities are presented in table 5.2. In the presentation of the results only slices z_1 to z_4 are shown. The remaining three slices have been added to better view a trend and to give a better insight in the three dimensional picture of the ice accretion on the geometry.

Property	Value
a	339.12 m/s
T	286.2 K
ρ	1.190 kg/m^3
U_∞	102.89 m/s

Table 5.1: *Flow properties for creating the 2D flow field of the propeller sections.*

Slice	z_1	z_2	z_3	z_4	z_5	z_6	z_7
$r[m]$	1.35	1.95	2.55	3.15	1.65	2.25	2.85
$U_{apparent}$ $[m/s]$	119.24	134.77	153.43	174.21	126.54	143.78	163.60

Table 5.2: *The slices in the z-plane and their distance from the center of the propeller blades as well as the apparent free stream velocity*

A flow field has been created for each of the slices. As the geometry of the blade is fairly curled, all sections need their own mesh. In figure 5.1 the necessity for this is clearly visible as the geometry curls along with the apparent flow for the relative sections on the propeller blade. This is a slight indication that this approach could be right. The geometry also gets thinner on the outer parts of the blade, causing less distortion of the flow. But as also visible in table 5.2, the apparent velocity increases significantly.

With this flow fields, the results have been examined using *Multi-Ice*. Firstly shown are the trajectory plots for the different sections. In figure 5.2 the trajectories corresponding to the flow field are shown. These show the trajectories of the droplets which will collide with the airfoil section. The two outer trajectories are also displayed, showing the first droplets that will not hit the propeller blade. In figure 5.2(d) there is a strange sudden angle in this outer trajectory. But as the droplet on this trajectory line do not influence any of the icing results it is left in.

Now that the trajectories of the droplets are known, it is also desired to know how much water is actually impinging the propeller blade. To do so, the β-coefficient is checked. This shows is an impinging factor of the droplets on the different sections. The plot in figure 5.3(a) shows the impinging factor for the slices z_1 to z_4. What can be seen from this plot, is that further outwards on the propeller, more droplets are impinging the profile. This could be explained by the significantly higher velocity the section experiences on these outer regions. The reason why slice z_4 has a much thinner collection span than the other three is

mainly because the geometry itself is also much thinner. Therefore, the leading edge is as well. Visible is however, that the impinging factor is much higher on this smaller surface. What can even been seen in slice z_3 and z_4 is that in some regions, the factor is above 1. This is odd, as it means more water is impinging than present in the trajectory line. A possible explanation is that water from different trajectories are impinging on the same locations, resulting in more water than would be present in one trajectory of air. Putting this all together, it can be seen that for an increasing velocity the impinging factor increases as well. Even resulting in more water than to be expected initially.

A bit more chaotic is the plot of the ice thickness of the different sections in figure 5.3(b). As can be expected from the β-coefficient plot, the ice thickness is largest on the outer slices. Due to the amount of water impinging the most ice will also be created here. The shape of the plots all describe a horn on the leading edge. With locally less ice on the on both sides of the stagnation point. The thickness corresponds to the shown shapes in figure 5.4. This shows that the horns are becoming not only larger in size, but also more rounded towards the outer edge. While looking closer to the shape of the ice on each section, it is very well possible that the ice would gradually build up in the given shapes for the sections. Apart from the horn on the leading edge, there is no ice present on the propeller sections. When looking at figure 5.5, the values from the ice thickness on the sections for all seven slices have been numerically integrated, calculating the volume of ice per span. The figure shows a nearly linear increase on the middle sections ($r = 1.95$ to $r = 2.85$), in these sections the geometry is quite similar. Meaning the ice accretion is indeed stronger for higher velocities. The highest section(s) show a decrease in ice volume, which is a result of a smaller geometry to impinge on.
For the ultimate comparison, the three dimensional geometry of the propeller blade, as used, has been plotted in figure 5.6. On this three dimensional mesh, the ice horns are added in their corresponding height. This means the geometry of ice seen on the blade is in scale with the propeller.

A point of discussion for the analysis of the ice accretion is that the programmed code in *Multi-Ice* does not cope well with high velocities and high temperatures. In these simulations, the temperature is set sufficiently low at $244K$. But the Mach number of the apparent velocity of the most outer simulated section is 0.48. This is very high and could result into ice breaking off, which is not embedded into the numerical solution. Also, in literature Tan and Papadakis , found that droplets impinging at high velocities have a greater rebound of the (iced) airfoil. Meaning it is possible that the impinged droplets do not all freeze to the surface as *Multi-Ice* thinks it does. However, to be able to confirm this, experimental data is needed as current icing software cannot handle these physical properties of the droplets. Also, little is known about the exact influence of the Mach number to these physics. [17] [18]

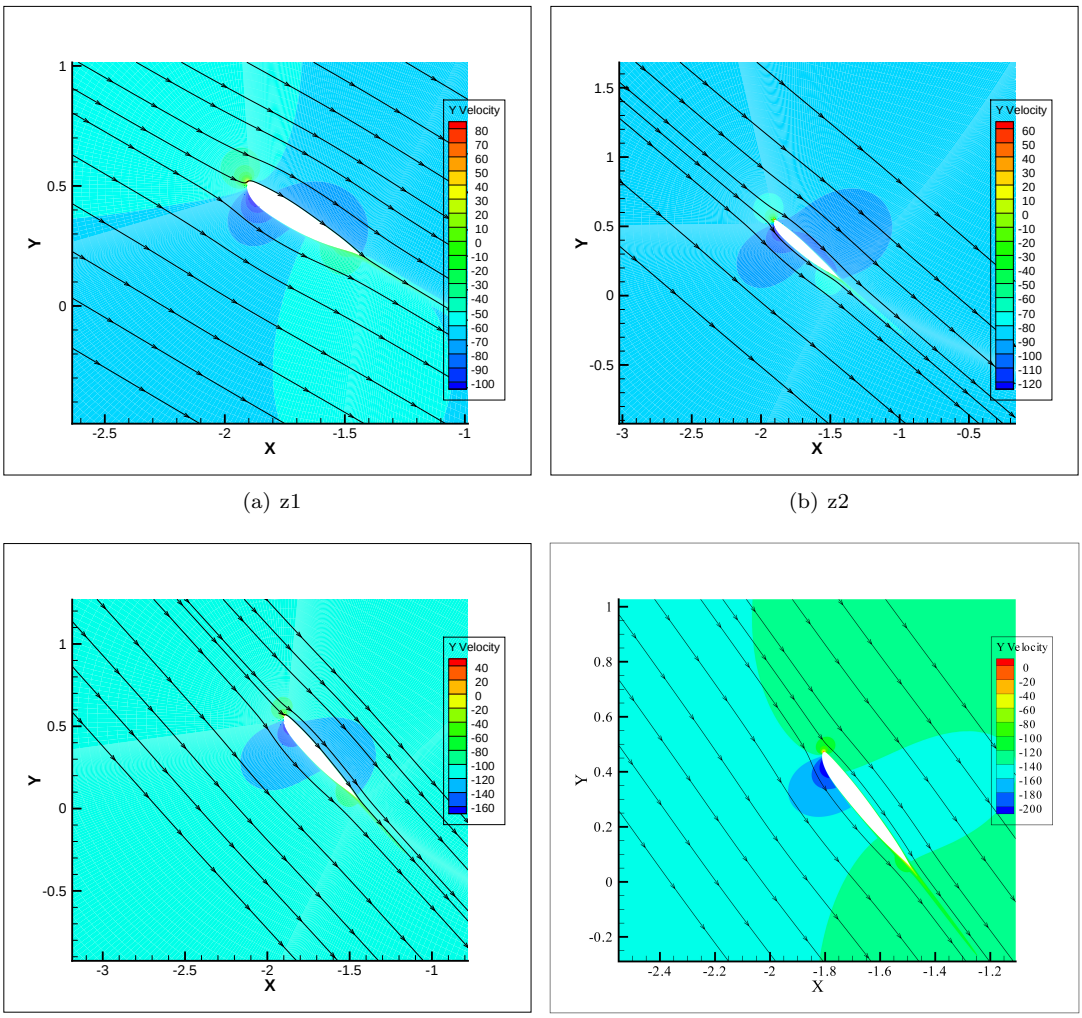

(a) z1

(b) z2

(c) z3

(d) z4

Figure 5.1: *Steamlines of the flow field and the Y-velocity, with conditions used as presented in tables 5.1 and 5.2.*

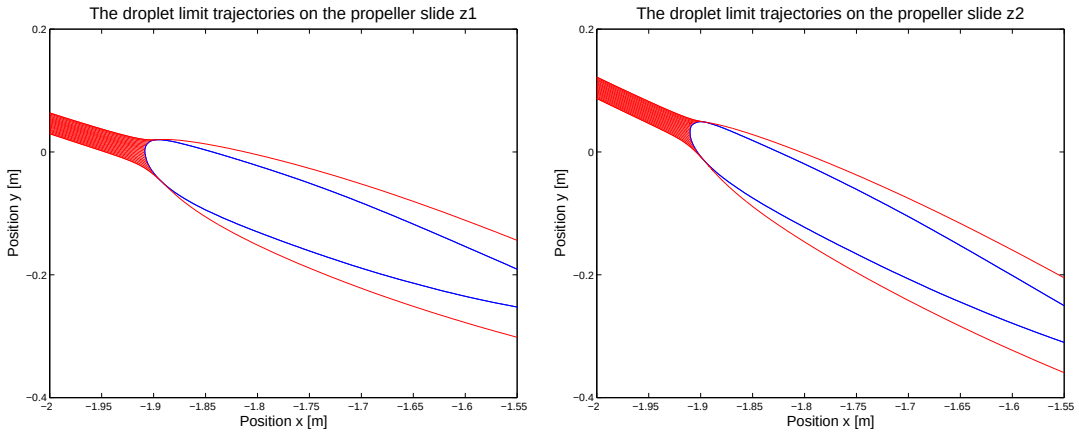

(a) z1

(b) z2

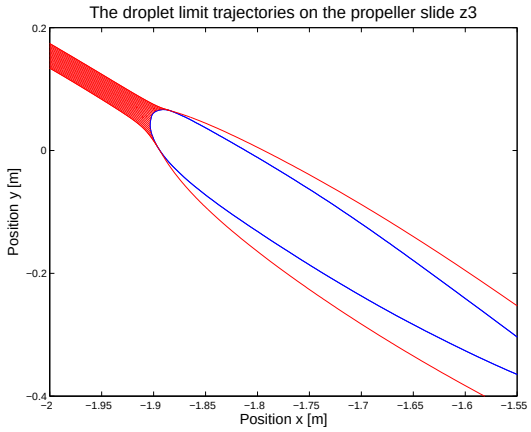

(c) z3

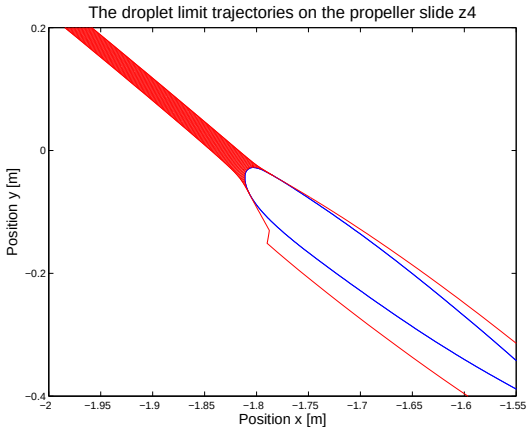

(d) z4

Figure 5.2: *The droplet trajectories for the different sections. (Flow conditions tables 5.1 and 5.2.)*

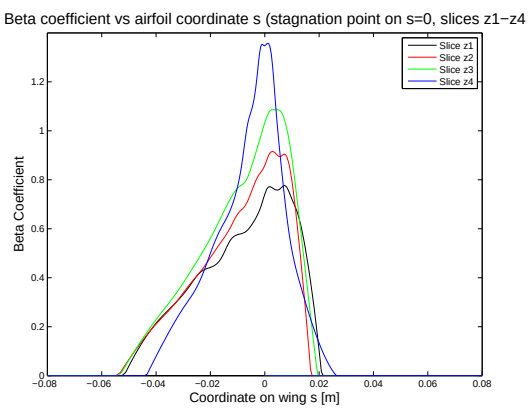

(a) Beta coefficient

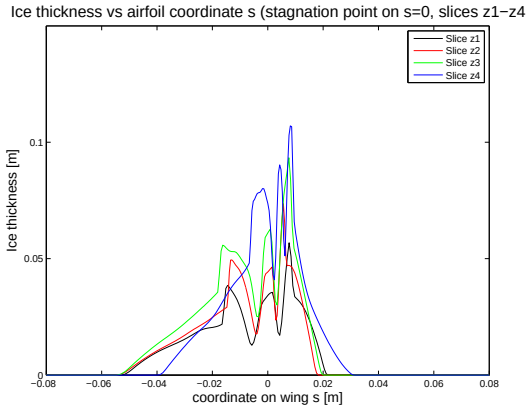

(b) Ice thickness

Figure 5.3: *The beta coefficient and Ice thickness on the coordinate of the airfoil with s=0 is the stagnation point.(Flow conditions tables 5.1 and 5.2.)*

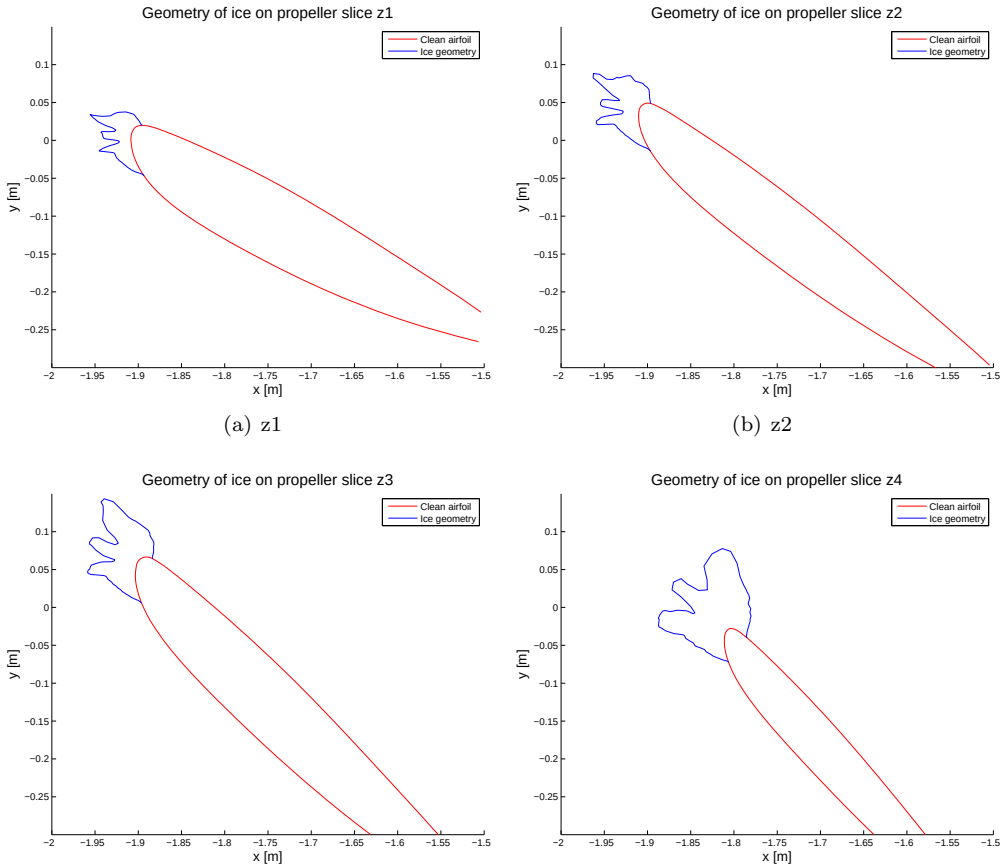

(a) z1 (b) z2

(c) z3 (d) z4

Figure 5.4: *The shape of the ice accretion on various slices among the propeller blade (Flow conditions tables 5.1 and 5.2.)*

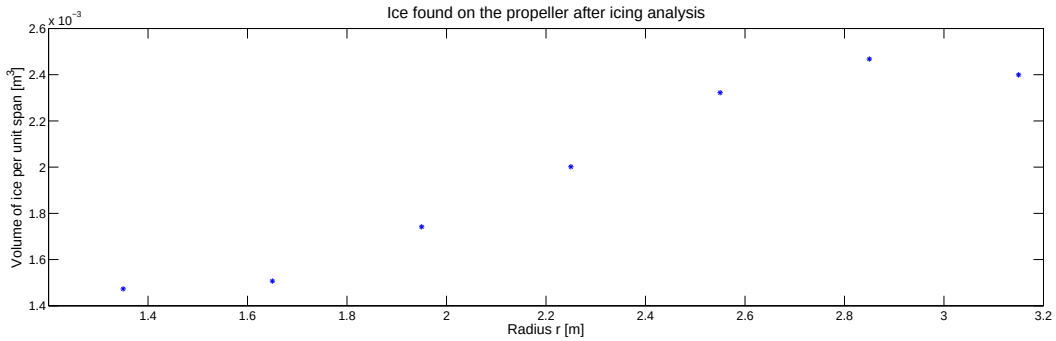

Figure 5.5: *The integrated values of the ice thickness along the s-coordinate (figure 5.3(b)).*

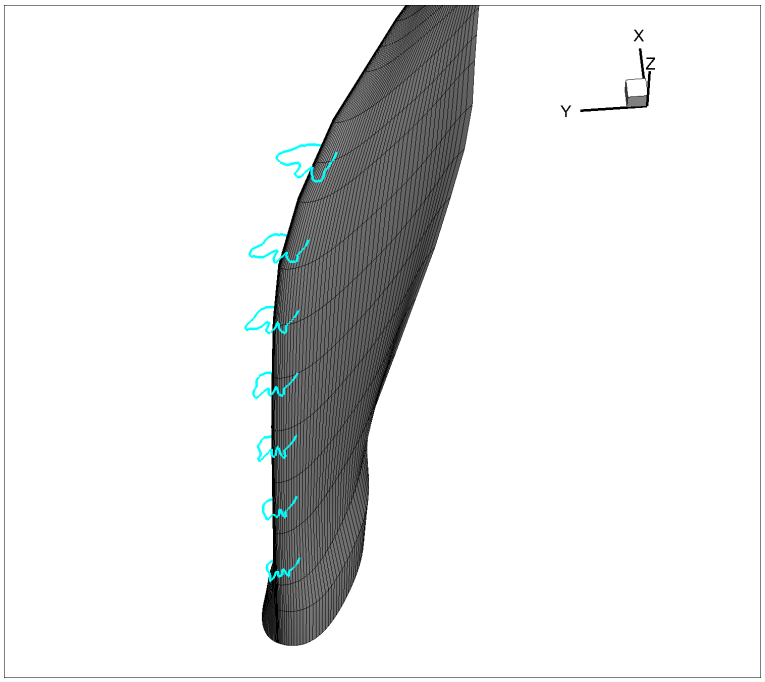

Figure 5.6: *Three dimensional plot of the ice build up along the leading edge using slice 1 to 7*

Anti-Ice analysis

The ice accretion on the propeller blade from this study is dangerously high and will most definitely decrease its performance significantly. This means the propeller needs to be protected from flying in the conditions analysed. In the literature study it is found that the most common and easy anti-icing system on a propeller blade is by heating it with an electrical path. Since there is a different amount of ice accretion for each section of the blade as previously studied, for each section an anti-icing analysis has been made. This will give an insight in how much energy is needed to clear the whole propeller of ice.

To show how such an analysis has been performed, the in-between data to get to the final design of the anti-icing on the first slice (z_1) has been presented. To obtain the data, the simulations for the ice accretion have been re-used. Then on the surface where ice is present, an (electrical) heat is added of a certain amount of W/m^2. *Multi-ice* does not simulate a flow of water on the profile, the water that does not freeze to the propeller will stay on the same location, resulting in a relatively thick layer of runback water. When no heat is added to the regions with water, the water will then freeze to the next point as the temperature of the propeller is still below the freezing point. Therefore, it has been decided to only clear the leading edge plus 15% of the chord length. This is assumed sufficient, but it can only be validated with the use of experiments. To define the leading edge, the original section containing ice has been used. So 0.15 m away (along the airfoil coordinate s) from the point where ice was first found will be the point where ice may build up in this numerical simulation.

In the graph in figure 5.7 the different tests to obtain the ice free leading edge using as little energy as possible are shown. Firstly, a constant value of $100,000\ W/m^2$ (*test1*) has been applied everywhere until 0.15 m away from where the ice originally formed. The results of the ice thickness and the runback water are shown in figure 5.8. Here it is clearly visible that the ice is practically gone. The thickness is below a measurable level (the black line is not even visible). Also, looking ahead, in figure 5.8(b) can be seen that some water even evaporates with this heat as much less water is present in test 1 than the other simulations. If more ice is melted, water should increase, as for evaporating the water too much energy is added. So for the second run, still a constant power was applied, but now $80,000\ W/m^2$ (*test2*). This power clears most of the ice, except for one peak near the stagnation point. This means more heat must be applied there, not as much as *test1* but just enough. The rest of the section might be able to still be ice-free using less power. For the third test shown, a peak of power is presented near the point where the remaining ice was found during *test2*. Moving away from this peak the applied power drastically drops

and eventually will go to zero at the point where the ice is allowed again. In the third to fifth (and final) presented series, the power curves have been slightly adjusted, such that the ice will form behind the marked 15% zones. As visible, each simulation the ice moves further away from the leading edge, whilst also attempting to use minimal power.

Now for the six other slices (z_2 to z_7), the same kind of analysis has been made. The results of slice z_2 to z_4 are presented in the figures 5.9, 5.10 and 5.11. What stands out from these figures is that on the upper side of the leading edge on all geometry sections, the largest power is applied in the form of a peak. This power then rapidly declines and remains constant with a slight decrease for the remaining part of the desired ice free zone. It was shown in the previous section that the amount of ice build up is increasing towards the outer part of the propeller blade. However, the simulation shows that the required power to prevent icing from occurring does not have a direct relation to the amount of ice. This is due to the fact that not only the amount of ice built up determines how much power is needed to keep it clean. The geometry and corresponding velocity will also influence these results. In table 5.3 the amount of power added per section is checked by integrating the graphs of the power density over the s-coordinate. The amount of power per slice does not follow any particular trend, but is fairly constant around 15000 W/m.

Slice	z_1	z_2	z_3	z_4	z_5	z_6	z_7
Power added $[W/m]$	15546	15286	15503	15700	14383	15561	14468

Table 5.3: *The amount of power to be added in one slice*

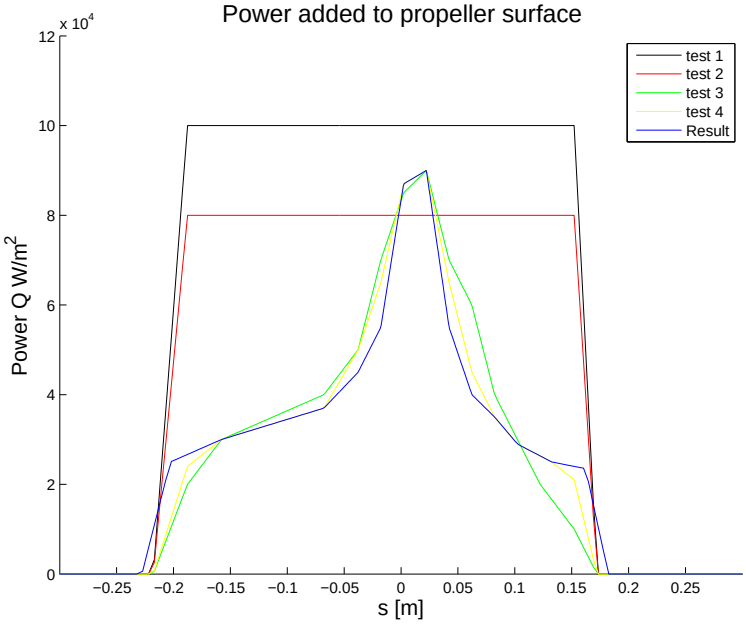

Figure 5.7: *Applied power to the propeller on slice z_1 per square meter*

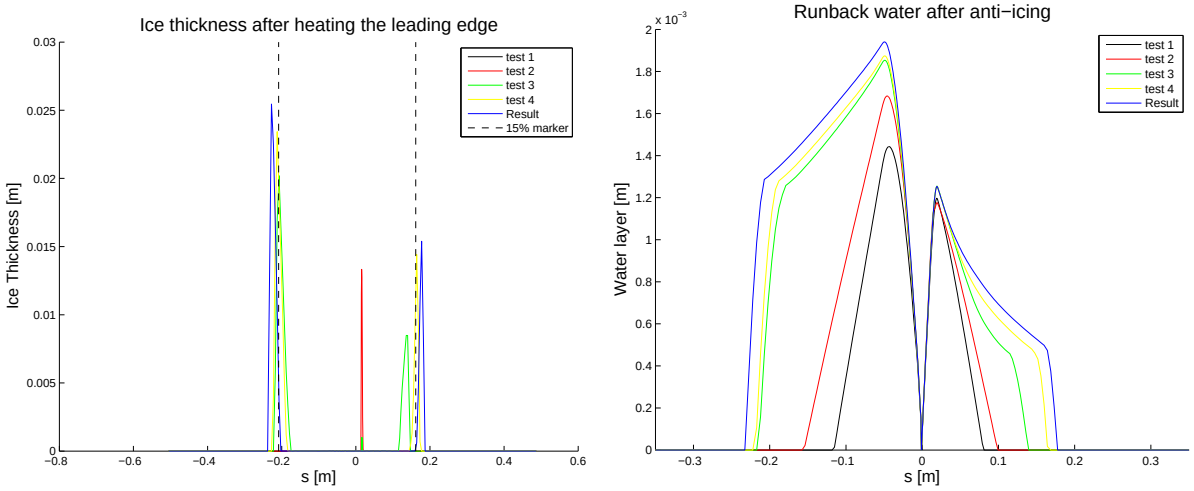

(a) Resulting ice (b) Runback water

Figure 5.8: *The ice thickness for several simulations of anti-ice set-ups for slice z_1.*

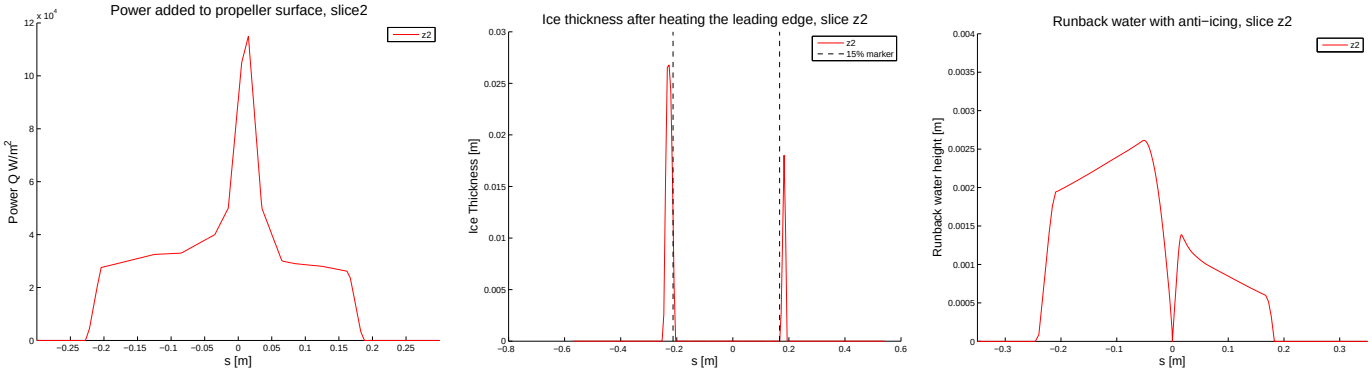

(a) Power density (b) Ice thickness (c) Runback water

Figure 5.9: *Anti-icing results for slice z_2*

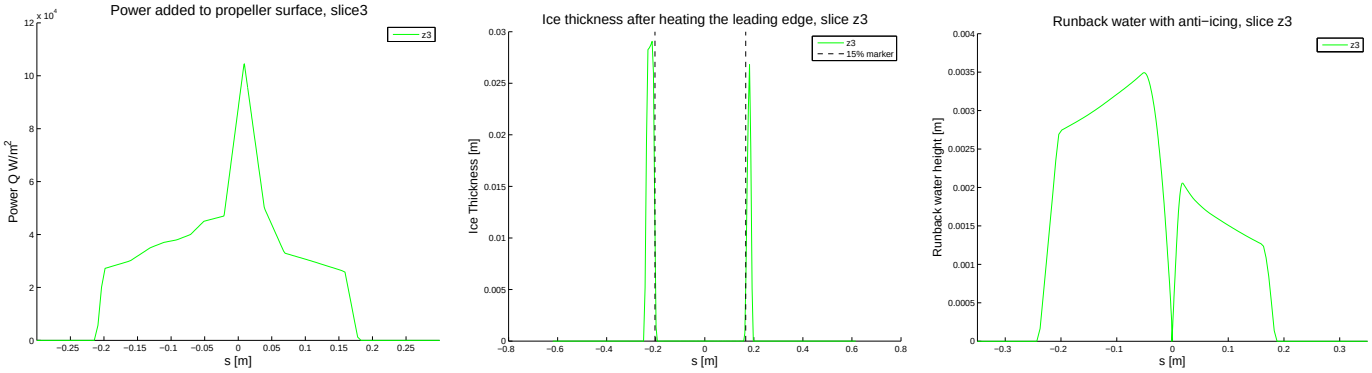

(a) Power density (b) Ice thickness (c) Runback water

Figure 5.10: *Anti-icing results for slice z_3*

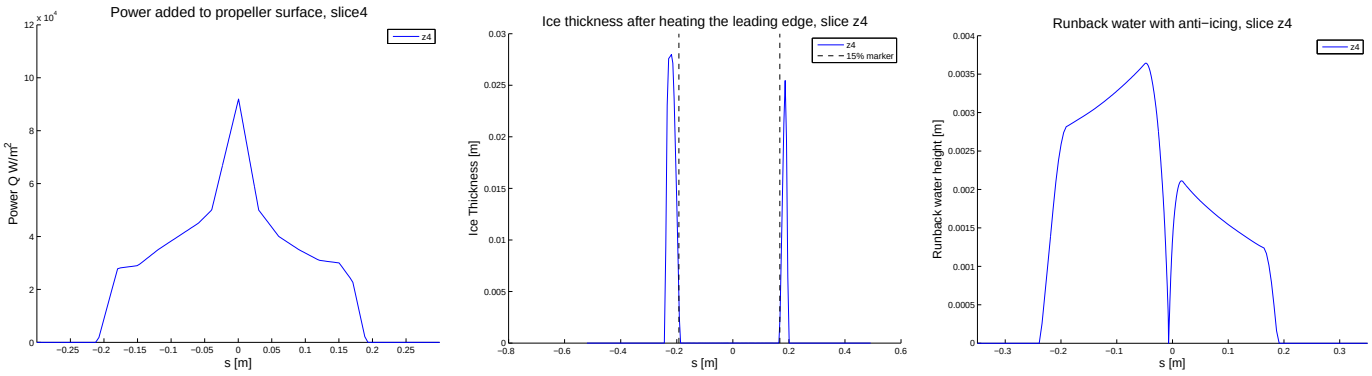

(a) Power density (b) Ice thickness (c) Runback water

Figure 5.11: *Anti-icing results for slice z_4*

To check if indeed all the ice was cleared of the propeller sections, and the water is not vaporised by the added heat, the plots of the total runback water on the four main sections have also been presented, next to the remaining ice residue sufficiently far from the leading edge.
Resulting from the anti-icing study is that the droplets impinging now form water instead of ice. To see how much water stays onto the propeller, these results per section are also added. Moreover, the remaining ice which supposedly forms after the heated section, is included as well. To see if the leading edge is indeed ice-free. These lines have also been integrated numerically and the resulting water and ice per section are plotted in figure 5.12. What can be concluded from this graph, is that with the heat in each section, the amount of runback water follows the exact same trend as the amount of ice (as presented in figure 5.5). To check if this result could be indeed valid, also the remaining ice has been plotted into the figure and it shows that this is a constant volume of ice present in all simulations. So it looks like the applied power to each section is appropriate.

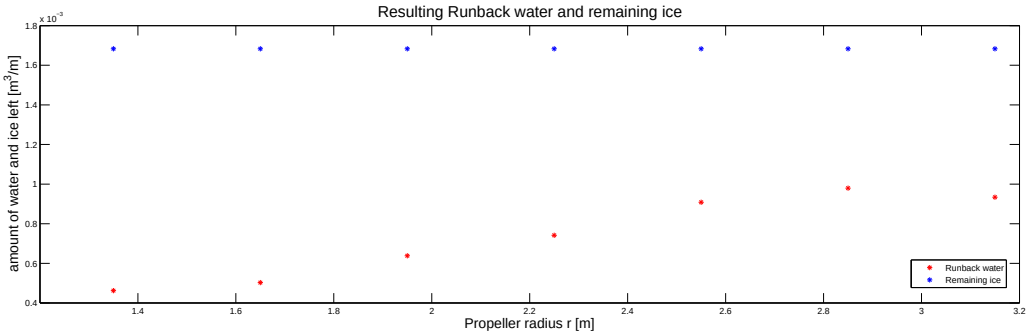

Figure 5.12: *The resulting runback water per section and remaining ice far from leading edge.*

Lastly, the added power of each section has been interpolated onto the three dimensional blade for a visualisation. Here it indeed visible that in the middle of the propeller the highest power is applied. The leading edge is heated about the same width everywhere. The interpolation is however not perfect in radial direction, as the mesh on which is interpolated is very coarse here. But the general picture is clear.

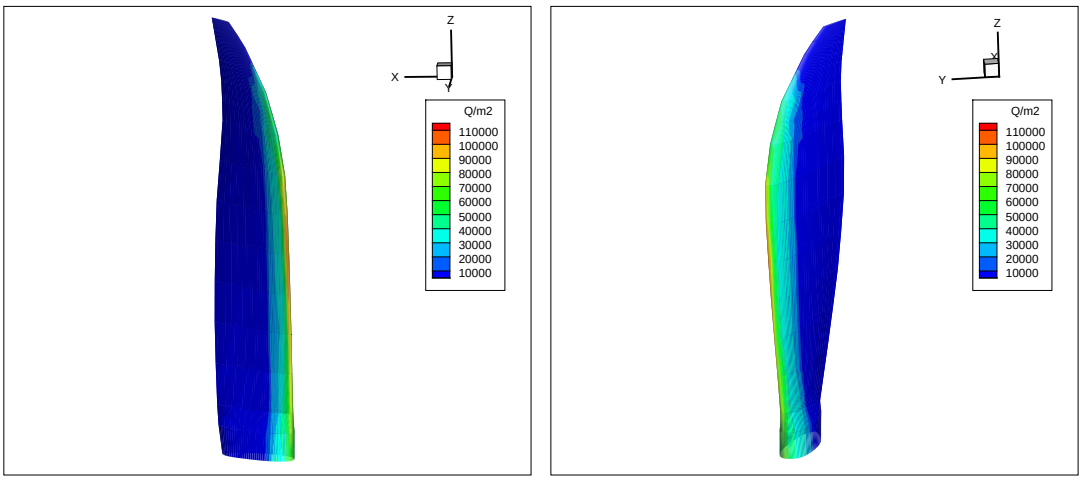

(a) 3D plot

(b) 3D plot inverse angle

Figure 5.13: *Interpolated values of the power density of the 7 slices visualised on a three dimensional profile*

6. Three dimensional check

It has been said before that the simplifications made must be validated to ensure that the simulations are a representation of the actual flow around the propeller. As there is no experimental data available to validate the flow field and icing analyses made in the previous chapters, a numerical three dimensional flow field is used to see if the local two dimensional analyses are valid.

The three dimensional flow field obtained has a slightly different geometry than that of the earlier simulations. Also, different slices have been used, but this should not influence the result much, as the previous analysis showed that the geometry of the ice is quite similar but for the volumes of ice. In the two dimensional analyses it was assumed that the far field velocity would consist of two velocity components. These components are the free stream velocity of the plane and the velocity induced by the rotation. The latter is measured by multiplying the radius times the rotational speed. The graphical representation of the apparent velocity was shown in figure 4.5. The velocity component is the radial direction was neglected as this was assumed to be minimal, especially in the mid-sections of the propeller. This is known to be the case close to the propeller. However, it might not be the case for the droplets moving in from further away. Therefore, it needs to be checked if the droplet trajectory / flow streamline will be following this assumed apparent velocity as they approach the propeller.

This flow field has been generated in slightly different flow conditions than the earlier simulations. The properties of the flow are presented in table 6.1 For the analysis of this three dimensional flow field, four slices have been used. The three extra slices in the two dimensional analysis are a good comparison to find a correlation between the radial differences. Unfortunately, there is not enough time to analyse them as well. The properties of the slices analysed are presented in table 6.2.

Property	Value
M	0.4
T	249.19 K
ρ	0.6601 kg/m^3
U_∞	126.57 m/s
Ω	44.67 rad/s

Table 6.1: *Flow properties for the creation of the 3D flow field (figure 6.1) of the propeller sections.*

Slice	z_1	z_2	z_3	z_4
r $[m]$	1.2	1.8	2.4	3.0
$U_{apparent}$ $[m/s]$	138.4	150.9	167.4	186.5

Table 6.2: *The different flow properties of the four slices.*

In figure 6.1 the streamlines constructed from the absolute velocity (x, y, z) directions is viewed in an Y-Z-plane. Also, the contour plot on the background shows the local values of the velocity in radial direction. Close to the propeller, the radial component of this velocity indeed approaches zero. Moreover, the streamlines show an full agreement with the assumption made in the earlier analysis. The flow approaches the propeller in a tangent angle, sufficiently far away from the airfoil to make the droplets travel in this direction as well.

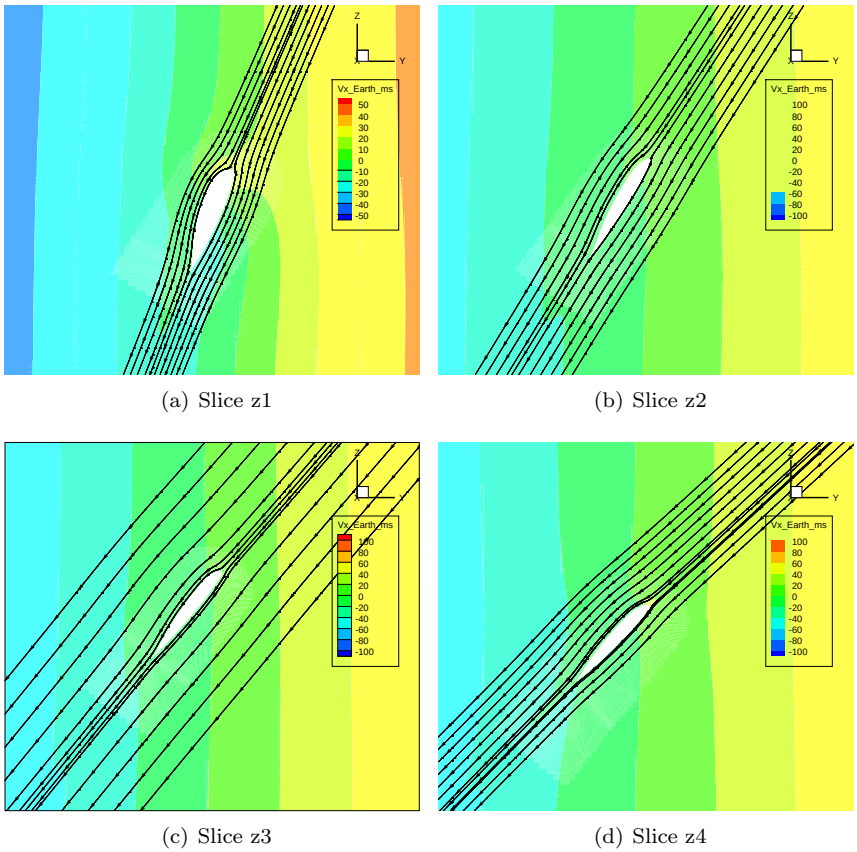

(a) Slice z1

(b) Slice z2

(c) Slice z3

(d) Slice z4

Figure 6.1: *The streamlines along the slices of the new three dimensional flow field.*

To be able to load the data into Multi-Ice, a flow from left to right is desired. Furthermore, the flows need to be normalised with their free stream apparent velocity (from table 6.2). Moreover, the program cannot handle three-dimensional input. Therefore, as the x-velocity component does not have influence on the streamlines for this section, it has been set to 0. Also, to be able to compare the flow slightly more to the earlier solution. In Multi-Ice, different settings regarding the temperatures have been set. These are still the same as the earlier computations, presented in table 4.2.

The simulations in Multi-Ice show that the ice has a different shape compared to the earlier computations. It is less horn shaped as the earlier simulations. Please note that as the flow field was given in dimensionless coordinates, in this case also the multi-ice simulations have been made in these dimensionless coordinates. This should however, not influence the results of the simulation. What is also visible in these plots is that for the first slice, in figure 6.2(a), the slice was chosen to be too close to the centre of the propeller set up. As this geometry catches significantly more ice then the others. This is also visible when plotting the accreted ice, similar to the earlier results (figure 6.3). This is the point where more simulations are necessary to be able to view a trend in the ice accretion. Assumed is that the trend is similar to the 2D analysis, only the geometry of the radius at 1.2 meter is too small, maybe here the three dimensional effect also plays a part. As visible in figure 6.1(a) the velocity in x-direction is between 10 and 20 m/s close to the leading edge.

Finally, the results of the full two dimensional analyses and the slices of the three dimensional field are compared. The flow fields consist of almost the same characteristics. The rotational speed of the propellers is almost equal. Unfortunately, the free stream velocity of the three dimensional field is much higher than the two dimensional free stream analysis. This could inflict some differences in the ice accretion as we already know that for high velocities Multi-Ice might not work perfectly. The stream lines in the three dimensional flow field and the two dimensional field show the exact same flow behaviour. As assumed the droplets appear to also follow the apparent velocity which was constructed from the rotational and free

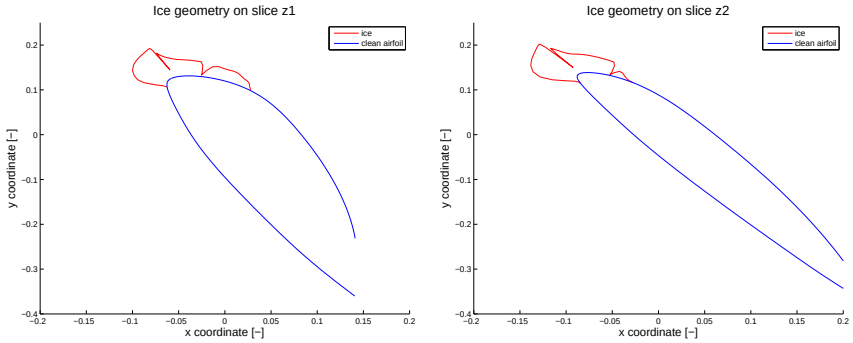

(a) Slice z1

(b) Slice z1

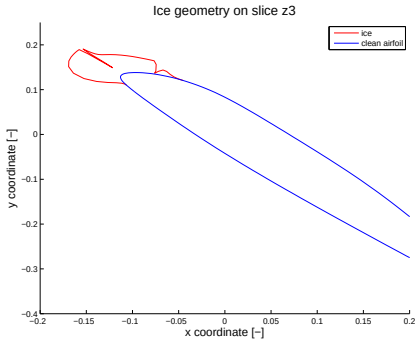

(c) Slice z1

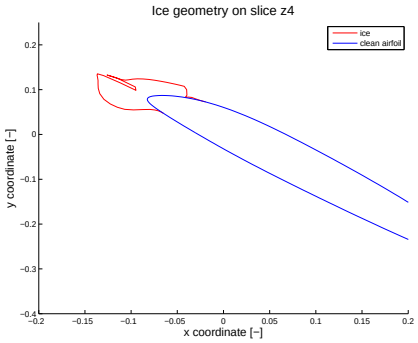

(d) Slice z1

Figure 6.2: *The ice geometry on the various slices.*

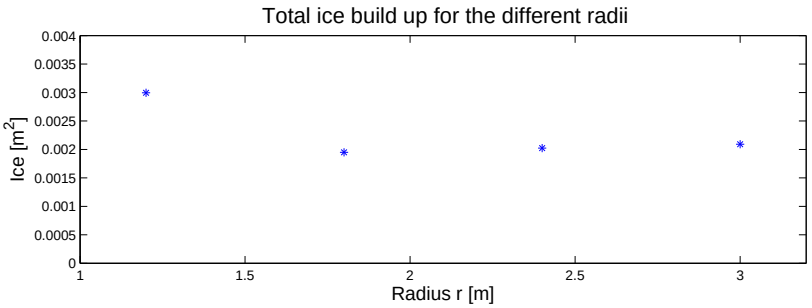

Figure 6.3: *The total ice build up for different radii*

stream velocity. The ice geometry of the three dimensional analyses are a bit odd and should be further researched.

7. Conclusion

The goal of this study was:

To perform an assessment of methods for propeller ice protection and to perform a case study for propeller ice accretion and ice protection design.

From the literature study, two solutions of propeller ice protection systems have been found. These are the weeping wing system, which distributes a freezing point depressant along the propeller. Using the centrifugal force to distribute it along the leading edge. With a large disadvantage that the it can only be used for systems where no bleed air is sent into the cabin. Because dangerous fumes may spread when these depressants are heated.
The second system, the system analysed, is the addition of electrical heating pads on the propellers leading edge. These heating pads can either heat the profile intermittently, to de-ice the propeller. Or continuously on a lower power, to keep the propeller clean of ice. The latter is further analysed using computational fluid dynamics.

After a few attempts for icing simulations on wings, an icing simulation was made for the propeller system as provided. Great difficulty was found in the obtaining of a proper flow field to describe a realistic flow. Therefore, an assumption has been made to use only the propeller geometry and simulate a flow using only the free stream properties as constants. An apparent velocity was constructed by combining the free stream and rotational velocity. This was done for seven different slices of the propeller geometry. To be able to gain an insight in the different levels of ice accretion. It showed that an increasing radius led to more ice. However, after the geometry started to get more slim near the tip, less droplets were caught, resulting into less ice accretion.

A three dimensional flow field was delivered which satisfies the Navier-Stokes equations. This is also analysed to try and compare if the assumptions in the two dimensional analyses were valid. It could be concluded that the flow field has identical properties. Also, for the mid-sections of the propeller geometry, the radial velocity component is nearly zero close by the propeller. For slices near to the nacelle and the propeller tip this is not the case. The assumption for the two dimensional flow is therefore only valid for a limited section of the propeller geometry.

On the ice found in the two dimensional analysis, an anti-icing analysis has been conducted. It became clear that to keep the propeller clean of ice, a power peak is necessary near the stagnation point of the geometry. Also, independent of the section and amount of ice built up on the different sections. All slices needed about the same amount of total energy, which was 15 kW/m. This is a value similar as seen while looking at suppliers of these anti-icing systems.

Unfortunately, this research has some flaws which can be better evaluated in a further research. The flow conditions of the two dimensional analysis are not equal to those of the three dimensional analysis. They were based on an earlier given three dimensional flow field, which appeared to be wrong. Therefore, it is strongly advised to simulate the two dimensional flow again with the same conditions as this will take less computing time. Furthermore, the icing results should be validated with the use of experiments, to ensure that Multi-Ice predicts the ice accretion correctly.

Bibliography

[1] I. Paraschivoiu and F. Saeed. *Aircraft icing*. Wiley-Interscience publication, 2004.

[2] Air owners and pilot association. Aircraft icing. `http://flighttraining.aopa.org/pdfs/SA11_Aircraft_Icing.pdf`.

[3] Scott K. Thomas, Robert P. Casoni, and Charles D. MacArthur. Aircraft anti-icing and de-icing techniques and modeling, 1996.

[4] James P. Lewis. *De-icing effectiveness of external electric heaters for propeller blades*. Flight Propulsion Research Laboratory, Ohio, 1948.

[5] Anti-ice and deice systems. `http://www.aboutflight.com/handbook-of-aeronautical-knowledge/ch-6-aircraft-systems/anti-ice-and-deice-systems`, 2015.

[6] R.B. Rutherford. De-ice and anti-ice system and method for aircraft surfaces, February 27 2001. US Patent 6,194,685.

[7] UTC Aerospace Systems. Icing conditions appendix c.

[8] C. Dumont, P. Pellicano, T. Smith, and J. Riley. Results from a full-scale propeller icing test. In *46th AIAA Aerospace Sciences Meeting and Exhibit*, 2008.

[9] FAR (Federal Aviation Regulations). Icing conditions appendix c, 2015.

[10] C. Dumont, P. Pellicano, T. Smith, and J. Riley. Propeller icing tunnel test on a full-scale turboprop engine. 2010.

[11] B.W. Corson, Jr. and J.D. Maynard. The effect of simulated icing on propeller performance. 1946. NACA TN-1084.

[12] G. Busch, M. Bragg, and A. Broeren. Prediction of propeller performance in icing conditions using vortex theory. In *1st AIAA Atmospheric and Space Environments Conference*, 2009.

[13] K.D. Korkan, L. Dadonet, and R.J. Shaw. Performance degradation of propeller system due to rime ice accretion, 1984.

[14] William B. Wright and Adam Rutkowski. Validation results for lewice 2.0, 1999.

[15] Inc ANSYS. Ansys fluent tutorial guide, release 14.0, 2011.

[16] Giuseppe Mingione and Francesco Petrosino. Cira multi-ice code version 3.3.3.

[17] S.C. Tan and M. Papadakis. Droplet breakup, splashing and re-impingement on an iced airfoil, 2005.

[18] Alan J. Bilanin. Proposed modifications to ice accretion/icing scaling theory, 1991.